Experiments with a Solid-Propellant Acoustic Oscillator

JOHN F. ENGLER*
Lockheed Missiles and Space Company, Sunnyvale, Calif.
AND
WILLIAM NACHBAR†
Stanford University, Stanford, Calif.

An end-burning, side-vented, solid-propellant motor has been developed to produce essentially one-dimensional acoustic oscillations. With use of a transparent quartz tube containing the propellant sample and serving as part of the combustion chamber during burning, direct measurement of unburnt length of propellant as a function of time is made with a high frame-rate motion picture camera and a Vanguard analyzer. Statistical analysis of the data shows that average burning rates can be determined to three significant figures with this technique. A typical experiment is described in which the acoustic oscillations in pressure, with frequencies of 1500 to 2000 cps and amplitude of 10 psi, are superposed upon a slowly oscillating mean pressure of nominal value 200 psia. Observed frequencies were some 20% less than frequencies calculated by one-dimensional acoustic theory for the equivalent closed-closed tube. Moreover, frequencies and amplitude of the oscillations were correlated with slow oscillations of mean pressure, decreasing pressure tending to increase amplitude and to decrease frequency. There was no measurable effect of the oscillations upon the average burning rate of the propellant.

Nomenclature

A = area, cm²
A_b = area of burning, cm²
b = linear burning rate, in./sec
$\bar{b}$ = average linear burning rate over web burning time
c = acoustic velocity, cm/sec
c^* = characteristic velocity, cm/sec
C_D = discharge coefficient
D = diameter, in.
f = frequency, cps
K_n = A_b/A_t, area ratio
L = length, in.
$\dot{M}$ = mass flow, g/sec
p = pressure, atm
R_2 = ideal gas constant, 82.059 atm-cm³/mole-°K
R_3 = ideal gas constant, 8.3144 × 10⁷ g (cm/sec)²/mole-°K
T = gas temperature, °K
t = oscillograph time scale, sec
t^* = film time scale, sec
W = molecular weight of total combustion products
γ^* = "shifting" gamma
θ = time scale correlation error, sec
ρ_π = propellant density, g/cm³
$\chi(\gamma^*)$ = see Eqs. (7) and (8)

Subscripts

c = "cold" end of gas cavity
F = film
h = "hot" end of gas cavity
i = initial (preignition)
N = nozzle plane
p = propellant
S = strand
t = nozzle throat

Statistical nomenclature

j = integer index $j = 0, \ldots, N$
$h(t)$ = a "hypothesis" for $b(t)$
N = number of data points
p^* = probability that a random F variable does not exceed F^*
$t_j \equiv t_j^* + \theta$
t_j^* = time at which unburnt propellant length is measured
$w_j \equiv W_j - \mu$, deviations of measured film length from least squares line
$W_j \equiv$ see Eq. (12d)
$X_j \equiv$ see Eq. (12a)
$Y_j \equiv$ see Eq. (12b)
$Z_j \equiv$ see Eq. (12c)
$\delta L_{pF}(t_0^*)$ = measurement error at $t^* = t_0^*$
μ = mean of the distribution of W_j
σ^2 = variance of the conditional distribution of w_j when given $-\delta L_{pF}(t_0^*)$
σ = standard deviation of the conditional distribution of w_j when given $-\delta L_{pF}(t_0^*)$

Superscripts

$\wedge$ = estimate

1. Introduction

THIS paper describes some results obtained with an end-burning, side-vented, solid-propellant motor designed to produce essentially one-dimensional acoustic oscillations. Other results are to be found in Ref. 1. The motor design is similar to that first reported by Horton and Ryan,[2] but with a number of modifications. Data reported here concern chiefly the burning rate during small-amplitude, self-excited pressure oscillations, the frequency of these oscillations, and the effect of mean chamber pressure on frequency and amplitude of oscillation.

An essential innovation in our experiments is the use of a transparent quartz tube that contains the propellant sample and serves as part of the combustion chamber during burning (Fig. 1). Direct measurement of the unburnt length of the propellant as a function of time is made with the use of a high frame-rate motion picture camera (16-mm Millikan, 400

Presented at the Acoustic Combustion Instability session (cosponsored by the Department of Defense Technical Panel on Solid Propellant Instability of Combustion) at the AIAA Solid Propellant Rocket Conference, Palo Alto, Calif., January 29–31, 1964 (not preprinted). The assistance of J. M. Lenoir during the initial experimental effort, of K. Berry in the subsequent experimental and computational portions of this work, and of B. E. Ellison in the area of statistical methodology are gratefully acknowledged.

* Senior Scientist. Member AIAA.
† Associate Professor, Department of Aeronautics and Astronautics. Member AIAA.

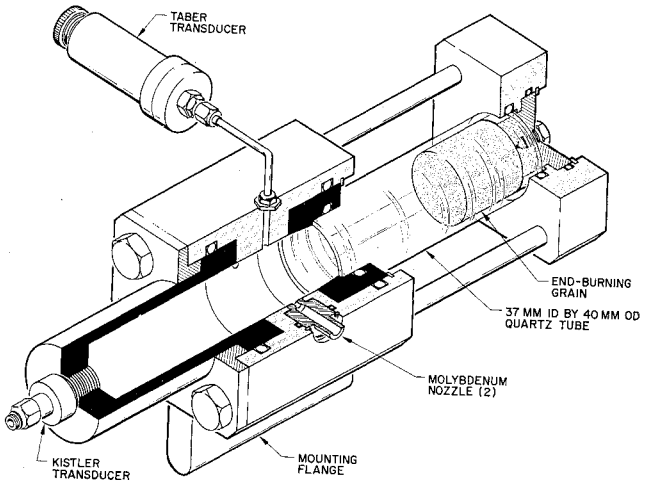

Fig. 1 Solid-propellant acoustic oscillator with transparent (quartz) combustion chamber.

frames/sec) and a Vanguard analyzer. A statistical analysis of the data, described briefly here but in detail in Ref. 1, shows that average burning rates can be determined to three significant figures with this technique.

2. Description of Experiments

The acoustic oscillator (Fig. 1) consists of three separable elements—the main body section, the hot-gas section, and the cold-gas section. The main body section is machined from 4130 steel, has an over-all length of 4.25 in., and contains two opposed nozzles machined from arc-cast molybdenum. The mean chamber pressure is monitored by a Taber transducer connected to a pressure tap located in the plane of the nozzles. This location was selected as it provides a means for determining when the pressure node was at the nozzle location.

The hot-gas section includes the transparent combustion chamber and the end-burning solid-propellant grain. The length of this section can be varied; however, for the experiments conducted to date, the distance from the nozzle plane to the end of the grain $L_{hi} + L_{pi}$ (Fig. 2) was either 5.6 or 6.1 in. The grains all had a diameter of 1.5 in. and a length of 1.0 in., giving a nominal burning time of 4 sec at an average pressure of 210 psia. The transparent combustion chamber is made of quartz with a nominal wall thickness of 1.5 mm and an internal diameter of 37 mm. Standard commercial quartz tubing proved to be an excellent structural material and safely withstood chamber pressures to 500 psia and theoretical flame temperatures to 2800°K. Frequencies as high as 2000 cps and peak-to-peak pressure amplitudes of 15% of the mean pressure had no observable effect on the structural integrity and strength of the quartz.

The success of a test when using the transparent tubes depends entirely on the nature of the contact of the propellant grain with the wall of the quartz tube. There can be no inhibiting material on the side of the grain, for carbon deposits would quickly smoke up the inside of the tube. However, there must be absolutely no space between the propellant and the walls, or else hot gases will ignite the unprotected propellant.

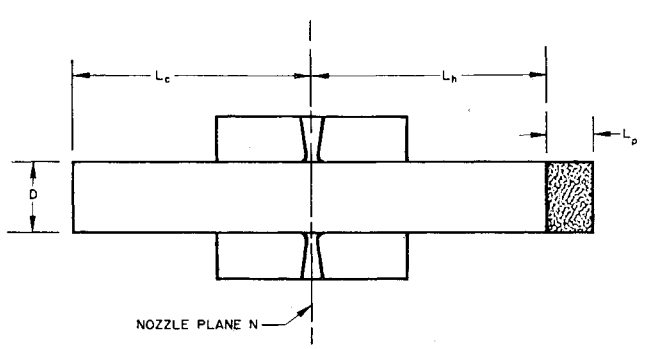

Fig. 2 Schematic diagram of acoustic oscillator.

The cold-gas section is a steel tube with a wall thickness of 0.18 in., closed at one end so that a pressure transducer (water-cooled Kistler PZ-18) can be mounted facing the propellant grain with the transducer diaphragm flush with the end wall. The length of this section can be adjusted, and the distance L_c from nozzle plane to the face of the transducer was varied from 0.80 to 6.48 in.

The igniter system consists of a small piece of propellant, generally weighing 0.5 g, which is wrapped in a piece of uninsulated manganin wire. This wire, in turn, is attached to two pieces of small-diameter, insulated, copper wire that are threaded through the nozzles and connected to a d.c. power source. The acoustic oscillator is mounted in a vertical position on the test stand so that the igniter can be suspended over the center of the grain and approximately 0.5 in. away from the surface. A grid of tungsten wires placed in front of the propellant grain remains visible during the test and is used as reference points to measure the regression rate of the burning propellant.

The clock checks the over-all frame rate for each test, and variations in the frame rate during a test can be checked by using the timed light streaks that are placed on the film by an internal circuit of the Millikan camera. Both the clock and the light streaks are synchronous with the 60-cps power line frequency. Time on the oscillograph record is indicated by timing lines that are also synchronous with the 60-cps power line frequency. Hence, the oscillograph time scale is also a suitable time scale for a test run. The clock, camera, and oscillograph are started just prior to the test, and a flashbulb, which is placed in parallel with the igniter circuit and in view of the camera, fires when the igniter circuit is closed. It is convenient, for comparing oscillation start-up characteristics between different tests, to shift the actual time scale uniformly for each test, so that $t = 0$ in the shifted time scale is comparable to the actual time at which the first indication of chamber pressure is observed on the oscillograph. When reference is made to t in the following discussions, the shifted time scale appropriate for each test is implied.

The frequency of pressure oscillation and the mean chamber pressure are determined from the oscillograph record with a probable error of 1%, and the peak-to-peak amplitude of pressure oscillations is good within a probable error of 2%.

3. Data Reduction

In order to compare the measured frequencies of the chamber pressure oscillations with theoretical frequencies calculated from an acoustic theory, the gas cavity length $L_c + L_h(t)$ and the temperature distribution in time and in space along the cavity must be known. The determinations of $L_h(t)$ is discussed in Sec. 4. The current method for determination of temperature and acoustic velocity from the data will be discussed in this section.

For oscillation frequencies of the order of 10^3 cps, such as those obtained in the current series of tests, it is assumed that the chemical reactions in the propellant combustion products are sufficiently fast that this mixture remains in chemical equilibrium in the chamber even under oscillatory conditions. The combustion products constitute the resident gas at least in the propellant end of the chamber (L_h in Fig. 2) and in the nozzle. (The current design of the chamber, unfortunately, holds trapped air in the transducer end of the chamber during burning.) Under this assumption of chemical equilibrium, the instantaneous state of the combustion products can be determined by thermochemical equilibrium calculations.

Such calculations have been carried out[1] for the propellant formulation used which consists of 19% polyurethane, 80% ammonium perchlorate, and 1% burning-rate catalyst. The strand-test burning rate b_S was correlated by the equation

$$b_S = 0.352p^{0.368} \text{ in./sec} \quad (1)$$

for p (psia) in the range 100 to 400 psia. These calculations enable the acoustic velocity c to be determined from

$$c = (\gamma^* R_3 T/W)^{1/2} (\text{cm/sec}) \quad (2)$$

where γ^* is the so-called "shifting" gamma, which is computed as the partial derivative of the pressure with respect to density at constant entropy.

The calculated equilibrium gas temperature of 2802°K at a 200-psia chamber pressure is an upper bound on the gas temperature in the chamber. Lower actual temperatures are expected because the reaction products do not generally achieve chemical and thermodynamic equilibrium, and also because there are nonadiabatic effects, such as heat losses to the walls. Since no thermocouples were used in these tests to measure actual gas temperatures inside the chamber, the gas temperature in the chamber at the nozzle plane was calculated from measured values of the characteristic exhaust velocity c^* as follows[3]:

$$c^* = [(R_3/R_2)(pA_t/\dot{M})] (\text{cm/sec}) \quad (3)$$

Under nonoscillatory conditions (steady flow),

$$\dot{M} = \rho_\pi b A_b (\text{g/sec}) \quad (4)$$

$$c^* = (R_3/R_2) p/\rho_\pi b K_n (\text{cm/sec}) \quad (5)$$

where $K_n = A_b/A_t$. The actual slight deviation of K_n from the value $(D_p/2D_t)^2$ can be determined from examination of the burnout portion of the pressure-time curve. If c^* is known, the temperature T_N in the chamber at the nozzle plane then can be calculated[3]

$$T_N = (W_t/R_3)[\chi(\gamma_t^*) C_D c^*]^2 (°\text{K}) \quad (6)$$

Here $\chi(\gamma^*)$ is the function

$$\chi(\gamma^*) \equiv \gamma^{*1/2}[2/(\gamma^* + 1)]^{[(1+\gamma^*)/2(\gamma^*-)1]} \quad (7)$$

$$\doteq 0.378[1 + 0.6\gamma^*] \text{ for } (\gamma^* - 1)^2 \ll 1 \quad (8)$$

Actual rather than stagnation quantities were used in Eqs. (3, 5, and 6) because the Mach number of the flow in the chamber was 0.01 or less.

The principal uncertainties in the use of Eq. (6) are the values of C_D (which are taken to be unity in the present work) and of c^*. One of the advantages of using the quartz tube combustion chamber is that values of c^* can be measured directly during the test by means of the direct measurement of b.

4. Burning-Rate Measurement

A complete description of the behavior in the acoustic oscillator under dynamic conditions requires more experimental information than can be reliably obtained from the chamber-pressure vs time curve alone. If an essentially one-dimensional flow is assumed, the mass flow of combustion products from the propellant and the gas cavity length must be determined as functions of time. The instantaneous length $L_c + L_h$ of the gas cavity is the initial length of the cavity plus the time integral of the regression rate of the burning surface of the propellant. If the regression rate cannot be determined accurately as a function of time, the instantaneous length of unburnt propellant must be measured directly.

The mass flow from the propellant surface is given by Eq. (4). This equation assumes that there is no significant variation of b over the surface; however, A_b could vary during the test. Furthermore, $b(t)$ may not be determinable with any assurance from the measured pressure-time curve. It was surmised from examination of the burnout portion of the pressure-time curves that the burning surface in the oscillator was very nearly plane during the tests. Direct experimental evidence of this condition was obtained from an interrupted burning; the grain edges were sharp and well defined, and the surface was flat.

The Vanguard analyzer allowed viewing of a single frame under 15 × magnification; the image of the propellant length on the ground-glass screen was 10% larger than actual length. Measurements can be made between any two points on the ground-glass screen with a maximum internal measurement error of magnitude 0.0002 in. There are, however, other sources of error more significant than the internal measurement error. Thermal expansion of the film in the analyzer will cause errors unless time is allowed for the film to reach thermal equilibrium. Another source of errors is in the determination of the position of the gas-solid "interface." Trials of repeated measurement on the same frame were performed to assess the total external measurement error. It was concluded from these experiments that the maximum total error, the sum of both internal and external errors, was 0.0025 in. Ideally, the burning rate $b(t)$ can be determined as the time derivative of the unburnt propellant length L_p. Thus,

$$b(t) = -dL_p/dt \quad (9)$$

Since it is not possible to measure instantaneous burning rate by using a finite number of measurements, the derivative in Eq. (9) must be replaced by finite differences in a practical calculation. This calculation is further complicated by the presence of errors in the measurement of L_p. A statistical method for determining $b(t)$ from the observed data is now described.

The strand-law burning rate $b_S(t)$ for a test is defined to be the function calculated using the oscillograph record of mean chamber pressure as a function of time and the strand-test burning rate law [Eq. (1)], which gives burning rate as a function of pressure. The time t in $b_S(t)$ is the time as measured on the oscillograph, and $b_S(t)$ is defined only for the web-burning time. The average of $b_S(t)$ over the web burning time is called $\bar{b}_S$, the average strand-law burning rate. The measured lengths of unburnt propellant will be a function of time on the film time-scale. This "film length" is denoted by $L_{pF}(t^*)$. If the measurement of $L_{pF}(t_0^*)$ includes an error of undetermined amount $\delta L_{pF}(t_0^*)$, the integral of Eq. (9) can be written as

$$L_p(t) = L_{pF}(t_0^*) - \delta L_{pF}(t_0^*) - \int_{t_0}^{t} b(\tau)d\tau \quad t_0 \le t \le t_N \quad (10)$$

A "strand-law length" $L_{pS}(t)$ can be defined in a similar way as

$$L_{pS}(t) = L_{pF}(t_0^*) - \int_{t_0}^{t} b_S(\tau)d\tau \quad t_0 \le t \le t_N \quad (11)$$

If the quantities X_j, Y_j, Z_j, W_j are defined for $j = 0, \ldots, N$, as

$$X_j \equiv L_{pS}(t_j) - L_{pF}(t_j^*) \quad (12a)$$

$$Y_j \equiv L_{pF}(t_0^*) - L_{pF}(t_j^*) \quad (12b)$$

$$Z_j \equiv L_{pF}(t_j^*) - L_p(t_j) \quad (12c)$$

$$W_j \equiv Z_j - \delta L_{pF}(t_0^*) \quad (12d)$$

then Eqs. (10) and (12) can be manipulated to give the following equation:

$$W_j = -Y_j + \int_{t_0}^{t_j} b(\tau)d\tau \quad (13)$$

The variable Z_j is the error in measurement of unburnt propellant length from the film, but is not "observable." The

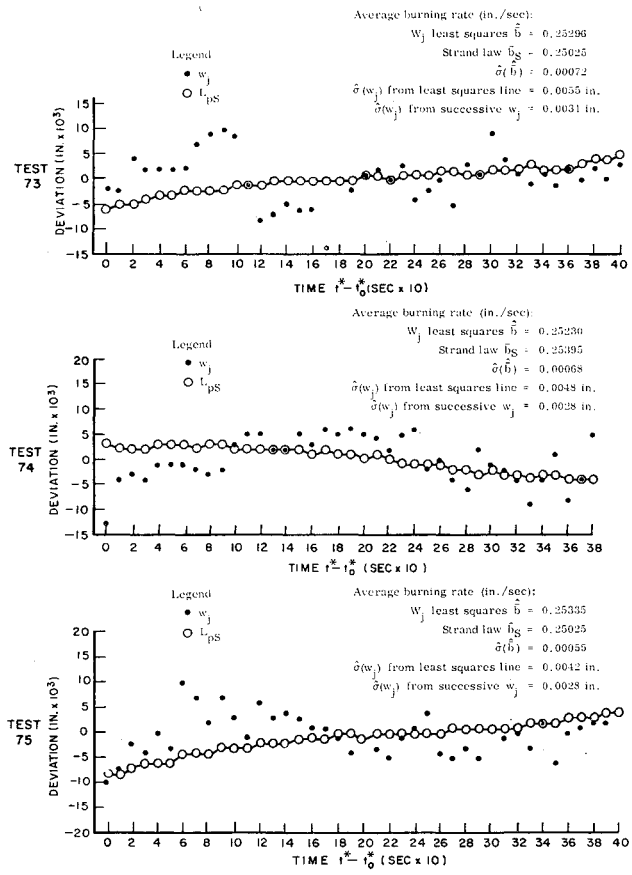

Fig. 3 Deviations from least-squares line fitted to L_{pF}, tests 73–75.

variable Y_j is directly observable from the film data; it should be noted that $Y_0 = 0$. The variable X_j is also observable, but depends upon the function $b_S(t)$. The quantity $\delta L_{pF}(t_0^*)$ is a constant for a given test but varies from one test to the next; it is an error in measurement independent of Y_j. Here, $Z_0 = \delta L_{pF}(t_0^*)$.

Equation (13) involves the correlation error θ implicitly in the limits of the integrals. If, for instance, $b(t)$ were a known function, then θ would also have to be known in order to compute W_j from Y_j by Eq. (12). In the statistical analysis given in detail in Ref. 4, θ is considered as a parameter to be estimated in the hypothesis for $b(t)$. A rough computation in Ref. 1 showed, however, that, for the present tests, θ is small enough so that neglecting it will not affect the results for $b(t)$.

The problem of direct determination of $b(t)$ from Eq. (9), in which case $L_{pF}(t^*)$ is used as an approximate measure of $L_p(t)$, is now replaced by another problem in which a function $h(t)$ is taken as a hypothesis for $b(t)$. A probability p^* (i.e., a number between zero and one) is to be obtained eventually from the observed data and will determine the compatibility of these data with the hypothesis $b(t) = h(t)$. Small values of p^*, e.g., $p^* < 0.05$, are regarded as unfavorable to the hypothesis, whereas larger values are regarded as tending to confirm the hypothesis. The functional derivation of p^* from the data is developed from statistical theory. A reasonable hypothesis for $h(t)$ is the strand burning rate $b_S(t)$. A more general hypothesis would be to assume that there is a constant departure from $b_S(t)$ during the test, and also that $b_S(t)$ may be shifted in phase from $b(t)$.

The procedure to test the hypothesis $b(t) = h(t)$ by determining p^* is based fundamentally upon an a priori estimate of the statistical distribution of the quantities W_j.

The following assumptions are made regarding W_j:

1) Conditional upon the value of $-\delta L_{pF}(t_0^*)$, for any test and for each j, these quantities are independent and identically distributed. This distribution differs from test to test only by translations due to the different values of $-\delta L_{pF}(t_0^*)$ from test to test.

2) Conditional only upon the value of $\delta L_{pF}(t_0^*)$, the unknown distribution is normal with unknown mean μ and unknown variance σ^2.

These assumptions regarding W_j follow reasonably from the hypothesis that the Z_j are independent errors of measurement, identically distributed. They imply, moreover, that σ^2 can be determined from Eq. (13) for a special group of tests in which $b(t)$ has a known functional form, and that this determination will suffice for all tests. This special group will be called the calibration tests for the oscillator.

5. Calibration by Nonoscillatory Tests

For calibration, a series of tests were made in which there were no acoustic-frequency oscillations. To achieve nonoscillatory operation while keeping all other significant variables fixed, the length L_c was decreased so that the nozzle plane was close to a pressure antinode for the fundamental longitudinal acoustic mode. Tests 73–75 were conducted under these identical conditions. Among these tests, the results on the oscillograph were indistinguishable.

For an ideally homogeneous propellant sample burning with a constant area of burning, the actual rate of regression of the visible edge of the surface during the web-burning portion of the test should be a function of the chamber pressue only, since all other parameters that affect this rate are expected to be constant. The pressure-time curves in tests 73–75 were sufficiently flat that significant departures of the measured burning rate from some constant value over the web-burning portion of the pressure-time curve can presumably be attributed to errors of measurement. The assumption is then made that

$$b(t) = \bar{b} = \text{const} \tag{14}$$

With reference to Eq. (13), therefore, the statistical model chosen provides that the mean of the random variable Y_j for each j is the linear function $\bar{b}(t_j^* - t_0^*) - \mu$, where, as previously noted, μ is the mean of the random variable W_j and is assumed to be independent of j. This is the standard linear regression model of statistical theory, and this theory is used to obtain point estimates of μ, $\bar{b}$, and σ^2, and confidence intervals for $\bar{b}$. Details of this theory are discussed in Ref. 4; it is sufficient to note here that the estimates of $\hat{\mu}$ and $\hat{\bar{b}}$ are obtained by applying least squares analysis to w_j, which is the deviation of W_j from its mean:

$$w_j \equiv W_j - \mu \tag{15}$$

From Eqs. (13–15), w_j is assumed now to be represented as

$$w_j = \bar{b}(t_j^* - t_0^*) - \mu - Y_j \tag{16}$$

The results of the calculations for tests 73–75 are shown by the curves in Fig. 3. For each of the tests, the computed value of $\hat{\bar{b}}$ is listed, together with the value of $\hat{\sigma}(\hat{\bar{b}})$, which, for each test, is an estimate of the accuracy of $\hat{\bar{b}}$ as an estimate of $\bar{b}$ for that test. From the small values obtained for $\hat{\sigma}(\hat{\bar{b}})$, it is seen that, in each test, $\bar{b}$ is estimated to within one digit in the third decimal place or third significant figure. Comparison of the estimate $\bar{b}$ from test to test shows that the values obtained on each of the tests are also in agreement to within one digit in the third significant figure. This last comparison has no statistical relation, however, to the values of $\hat{\sigma}(\hat{\bar{b}})$ and may in fact be fortuitous.

The values of $\bar{b}_S$ are computed as the average of b_S over the test (not as the value of b_S corresponding to the average chamber pressure). These three values follow the trend of the average chamber pressure for each of the tests. The differences between $\bar{b}_S$ and $\hat{\bar{b}}$ for the three tests are, respectively, -0.00271, 0.00165, and -0.00310. These differences

are considerably larger than $\hat{\sigma}(\hat{b})$. They are also much larger than could be accounted for by the reflection in $\bar{b}_S$ of experimental errors in the determination of chamber pressure.

The values of w_j computed from Eq. (16), with $\mu = \hat{\mu}$ and $\bar{b} = \hat{\bar{b}}$, are shown as dots on the graphs in Fig. 3. An estimate of the standard deviation of w_j is denoted by $\hat{\sigma}(w_j)$. The average among the three tests of the values of $\hat{\sigma}(w_j)$ is obtained from the least-squares line in 0.00483 in. It is observed, however, that this value is much larger than the expected maximum error in the measurement of L_{pF} which was found by experimentation to be about 0.0025 in.

Still another anomaly in these data arises upon visual inspection of the distribution of the w_j about the zero line. This distribution is equivalent to the distribution of Y_j about the fitted line $\hat{\bar{b}}(t_j^* - t_0^*) - \hat{\mu}$. If the underlying assumptions are all correct, the occurrence of positive and negative values of w_j should be random. However, points with the same algebraic sign are seen to occur in long sequences, the pattern of the sequences being different for each test. Furthermore, if all assumptions previously made were true, then another estimate $\hat{\sigma}(w_j)$ made from differences of successive values of the w_j (see Fig. 3) should be about equal (see Ref. 4) to the estimate made from least-squares line for each test. However, the average of the three values of the former estimate was only 0.0029 in. much less than the 0.00483-in. average of the least-squares estimates and much closer to the expected value of $\sigma(w_j)$.

6. Oscillatory Test Results

Information taken from the oscillograph record for a typical oscillatory test, test 69, is shown in curves 1, 3, and 5 of Fig. 4. All data have been plotted against a common and greatly reduced time scale so that the relationship between amplitude, frequency, and mean pressure can be seen more readily. It should first be noted that low-amplitude acoustic oscillations are associated with high frequencies and high mean pressures. When the amplitude increases, there is an accompanying decrease in frequency and mean pressure. In addition, all increases in amplitude are logarithmic with respect to time; however, a decrease in amplitude does not show such a relationship.

Curve 2 in Fig. 4 represents the pressure-time curve that would be observed for test 69 if the acoustic pressure oscillations were not present. This curve was constructed from data from the nonoscillatory tests. The data were modified to compensate for the slightly different burning area and propellant length, which were obtained in test 69. Curve 2 also reflects a c^* value of 4448 fps; this value was obtained from an average of the data obtained from the three nonoscillatory tests. A comparison of curve 1 in Fig. 4 with curve 2 shows a marked effect on the mean chamber pressure at the start of burning and a lesser though still significant effect throughout the balance of the test. This effect appears to be well-correlated with the amplitude of the acoustic frequency oscillations shown on curve 5.

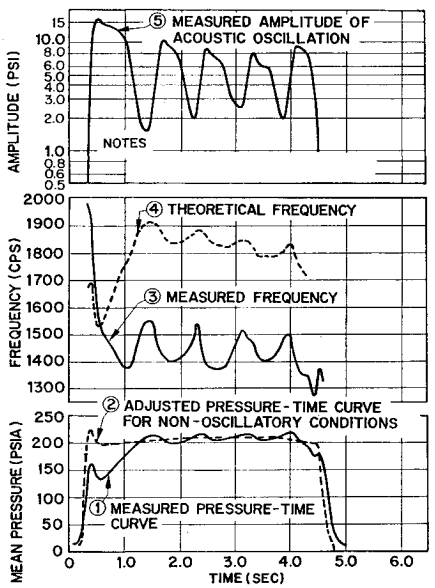

Fig. 4 Curves showing data from test 69.

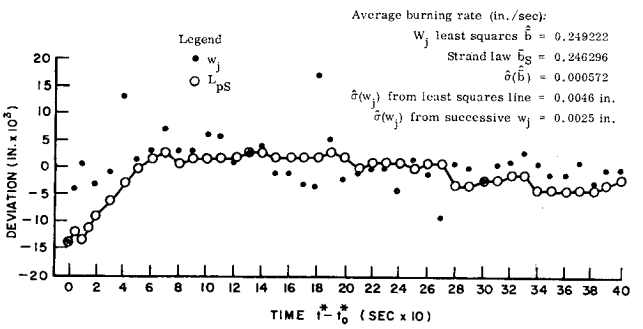

Fig. 5 Deviation from least-squares line fitted to L_{pF}, test 69.

In order to calculate the acoustic velocity and the gas cavity length for test 69 as functions of time, the relation between mean pressure and mean burning rate under oscillatory conditions must be determined. Even though the burning surface regression rate in the oscillator was found to agree with the strand law to two significant figures for nonoscillatory conditions (Sec. 5), it does not necessarily follow that this similarity will be true for oscillatory condition. The reduction and statistical analysis of the film data on $L_{pF}(t)$ for test 69 was carried out by means of the procedure previously described in Sec. 5 for the nonoscillatory tests. The values of w_j computed from Eq. (16) with $\mu = \hat{\mu}$ and $\bar{b} = \hat{\bar{b}}$ are shown as dots in Fig. 5.

The results for this test are seen to be indistinguishable from the nonoscillatory test results shown in Fig. 3. Such results may appear unexpected, since the pressure-time curve 1 of Fig. 4 shows an oscillation in chamber pressure of approximately 10 psi about the adjusted pressure-time curve 2 for nonoscillatory conditions. This oscillation could have been expected to produce an oscillation of the actual burning rate which, in turn, would be expected to show as a roughly sinusoidal trend in the values of w_j for increasing j (increasing time).

However, writing from Eq. (1) an expression for the change Δb_S in b_S caused by a small change in pressure Δp,

$$\Delta b_S/\bar{b}_S = 0.368(\Delta p/p) \qquad (17)$$

we find that, if $\Delta p = 10$ psi, $p = 210$ psi, and $\bar{b}_S = 0.2463$ are taken from test 69 as typical, the result is $\Delta b_S = 0.004316$ in./sec. Over one-quarter of a cycle, Δb_S will produce a variation in L_p of 0.001079 in., and this variation is considerably less than $\hat{\sigma}(w_j)$. This low-frequency, low-amplitude oscillation in pressure results, therefore, in an oscillation of the burning rate that is too small to be detected by the present technique for measuring L_p.

The solid line shown in Fig. 5 is the difference between L_{pS} and the least-squares line, $\hat{\bar{b}}(t_j^* - t_0^*) - \mu$, which was fitted to L_{pF}. This difference is calculated numerically as $w_j + X_j$. Lines similarly calculated for the nonoscillatory tests are shown in Fig. 3. The latter lines are essentially of constant slope, reflecting a very small, constant difference between b and b_S. Some oscillation is shown by the L_{pS} line in Fig. 5, but, in view of the sizable values obtained for $\hat{\sigma}(w_j)$, this oscillation is not regarded as significant.

It is concluded, therefore, that the actual instantaneous burning rate in this test agreed with the strand-law prediction to two significant figures. This result, for the quite small

amplitudes of pressure oscillation that prevailed in the test, is in agreement with the test results of Eisel.[5]

With use of the strand burning law, therefore, a theoretical frequency curve can be constructed (Fig. 4, curve 4) for the fundamental longitudinal acoustic mode of a closed-closed tube, assuming that the gas is uniform throughout the tube. Its shape is similar to the pressure-time curve, shown in Fig. 4 (curve 1), since c^* (and, consequently, gas temperature) is a function of pressure [see Eq. (5)]. For time greater than approximately 1 sec, the actual frequency (Fig. 4, curve 3) matches the theoretical frequency (Fig. 4, curve 4) in shape, but is lower by approximately 20 or 25%.

One contributing factor to this difference in frequency is that the gas temperature in the chamber is not uniform but is considerably cooler at the end away from the propellant, thus displacing the node toward that end. Consequently, the tube can be considered to have an effective length somewhat longer than the actual length. The gas temperature in the hot end can never be less than the average gas temperature for the entire tube (as determined by the c^* calculation) and can never be higher than the theoretical flame temperature. Without exceeding these limits, curve 4 can be adjusted downward to match the actual frequency curve (3) from 1.0 sec after start to the end of the test. This adjustment assumes that the pressure node is shifted toward the cold end and is placed at a point approximately one-third the distance from the cold end. However, the foregoing explanation is inadequate to account for the frequencies that occur at the onset of the oscillations (before 1.0 sec of test operation), and it is probable that these frequencies do not represent a closed-closed acoustic mode of operation.

7. Conclusions Regarding Burning-Rate Measurements

Experiments described in this report support the hypothesis that the actual burning rate $b(t)$ is equal to the strand-law burning rate $b_S(t)$ to two significant figures, at least at the low-amplitude levels of oscillatory burning observed in test 69. A surprising result, however, is the failure of the observed w_j to satisfy the plausible assumptions that were postulated in Sec. 4. This anomaly was not noticed at first by the authors, but was subsequently considered. The first approach to the statistical analysis of these data was to treat the w_j as a data sample without regard to the sequence that the data points follow in time. Considered as such, the sample cumulative probability distribution for each test was found to follow very closely the cumulative probability distribution for the normal distribution, and this close agreement was misleading. The basis for the analysis presented in this paper assumes that 1) for each value of j, each w_j is a sample from a normally distributed population, and 2) these values are uncorrelated in time. It is this second assumption that has been directly refuted by the data obtained from tests 73–75. Further, it is also possible that the first assumption is untrue.

If the first assumption is false, it would imply that, in at least one set of instruments and data recorders, the measurements were affected by a nonrandom distribution of measurement error. A typical example would be variation of the frame rate of the Millikan camera during the course of the test. However, all conceivable sources of such error have been closely examined, and no physical basis has been found for believing that there were any nonstochastic effects upon the measurements or the recordings.

If the first assumption is true but the second false, then the fault must lie with the assumption that $b(t)$ is absolutely constant during the calibration tests. It can be estimated from Eqs. (1) and (17) that fluctuations of pressure below a noise level of about 1% are utterly unable to account for the required variation of $b(t)$ from constancy. The present best guess is that nonhomogeneity of the propellant itself is the major cause of the time correlation of w_j. The term "nonhomogeneity" means, for example, nonuniform dispersion of the oxidizer or burning-rate modifier in the matrix and, also, the presence of nonpalpable voids. Before all tests, x-ray inspection of the grains was used to reject grains with obvious defects.

A rough indication can be given of the magnitude of the change in burning rate which could be due to nonhomogeneity and which would give rise to values similar to the observed means of w_j. If it is supposed that the principal component of the burning-rate spectrum of a nonhomogeneous propellant, burning at constant pressure, is a sinusoidally oscillating increment of burning rate with amplitude Δb_2 in./sec, frequency f_2 cps, and phase-angle θ, then, for the calibration test, the mean of w_j can be represented approximately as follows:

$$\Delta b^2 \int_{t_0}^{t_j} \sin(2\pi f_2 \tau + \theta) d\tau = \frac{\Delta b_2}{2\pi f_2} \Big[[\cos(2\pi f_2 \tau + \theta)]_{t_j}^{t_0} \quad (18)$$

If, from inspection of Fig. 3, $f_2 = 0.5$ cps is chosen, and the amplitude of the mean of w_j is taken as 4×10^{-3} in., then Δb_2 is given approximately as

$$\Delta b_2 = 2\pi f_2 \cdot 4 \cdot 10^{-3} = 0.013 \text{ in./sec} \quad (19)$$

Thus Δb_2 is crudely estimated to be about 5% of $\bar{b}$. This figure is not greatly different from the variations of the average burning rate in a strand-burner test for different sections of a strand-test sample. The possibility of a 5% fluctuation of the actual burning rate during a test at constant pressure in the oscillator does not seem unreasonable.

During oscillatory burning, $b(t)$ can probably be determined more accurately by the statistical model described in Ref. 4. However, this method requires that the distribution of $W(t)$ be known, and, probably because of the nonhomogeneity of the propellant, this distribution could not be determined with sufficient precision by our calibration tests. These results point to the necessity for strict tolerances on propellant nonhomogeneity if meaningful data are to be obtained.

References

[1] Engler, J. F. and Nachbar, W., "Experiments with a solid-propellant acoustic oscillator," Lockheed Missiles and Space Co., Rept. 6-90-63-80 (July 1963).

[2] Horton, M. D., "One-dimensional solid-propellant oscillatory burner," ARS J. **31**, 1596–1597 (1961).

[3] Emmons, H. W. (ed.), "Fundamentals of gas dynamics," *High Speed Aerodynamics and Jet Propulsion* (Princeton University Press, Princeton, N. J., 1958), Vol. III.

[4] Ellison, B. E., "Statistical methodology," Appendix C to Ref. 1.

[5] Eisel, J. L., "The effect of acoustic pressure on the burning rates of solid-rocket propellants," Fall Meeting, Western States Section, Combustion Institute, Paper 62-63, Preprint WSS/CI (November 1962).